Journal Pre-proof

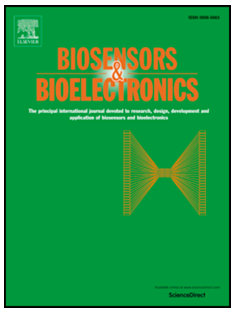

A new lateral flow plasmonic biosensor based on gold-viral biomineralized nanozyme for on-site intracellular glutathione detection to evaluate drug-resistance level

Hao-Han Pang, Yong-Chen Ke, Nan-Si Li, Ying-Tzu Chen, Chiung-Yin Huang, Kuo-Chen Wei, Hung-Wei Yang

PII: S0956-5663(20)30320-1

DOI: https://doi.org/10.1016/j.bios.2020.112325

Reference: BIOS 112325

To appear in: *Biosensors and Bioelectronics*

Received Date: 27 February 2020

Revised Date: 19 May 2020

Accepted Date: 22 May 2020

Please cite this article as: Pang, H.-H., Ke, Y.-C., Li, N.-S., Chen, Y.-T., Huang, C.-Y., Wei, K.-C., Yang, H.-W., A new lateral flow plasmonic biosensor based on gold-viral biomineralized nanozyme for on-site intracellular glutathione detection to evaluate drug-resistance level, *Biosensors and Bioelectronics* (2020), doi: https://doi.org/10.1016/j.bios.2020.112325.

Hao-Han Pang: Methodology, Software, Validation, Formal analysis, Investigation, Writing - Original Draft

Yong-Chen Ke: Methodology, Investigation, Formal analysis, Resources, Project administration.

Nan-Si Li: Methodology, Investigation

Ying-Tzu Chen: Methodology, Investigation

Chiung-Yin Huang: Project administration, Resources

Kuo-Chen Wei: Conceptualization, Project administration, Resources, Funding acquisition

Hung-Wei Yang: Conceptualization, Methodology, Project administration, Writing - Review & Editing, Supervision, Funding acquisition

A new lateral flow plasmonic biosensor based on gold-viral biomineralized nanozyme for on-site intracellular glutathione detection to evaluate drug-resistance level

Hao-Han Pang,[#a,b] Yong-Chen Ke,[#c] Nan-Si Li,[a,b] Ying-Tzu Chen,[a] Chiung-Yin Huang,[d] Kuo-Chen Wei,*[d] Hung-Wei Yang**[a]

[a] Institute of Medical Science and Technology, National Sun Yat-sen University, 70 Lienhai Rd., Kaohsiung 80424, Taiwan

[b] Institute of Biomedical Sciences, National Sun Yat-sen University, 70 Lienhai Rd., Kaohsiung 80424, Taiwan

[c] Department of Chemistry, National Sun Yat-sen University, 70 Lienhai Rd., Kaohsiung 80424, Taiwan

[d] Department of Neurosurgery, New Taipei Municipal TuCheng Hospital, Chang Gung Memorial Hospital and Chang Gung University, New Taipei City 23652, Taiwan

[#]H. H. Pang and Y. C. Ke contributed equally to this work.

Corresponding Author

*E-mail address: kuochenwei@cgmh.org.tw (K.C. Wei)

**E-mail address: howardyang@mail.nsysu.edu.tw (H.W. Yang)

Abstract

Temozolomide (TMZ)-resistant glioblastoma multiforme (GBM) cells would have abnormal redox status due to bio-thiols, like glutathione (GSH), which constitute the most crucial defense system that protects cells from therapeutic agents. Current strategies for GSH detection often require sophisticated instruments that may not be available in laboratories with fewer resources. Here, we circumvent this problem by introducing a lateral flow plasmonic biosensor (LFPB) based on gold-viral biomineralized nanoclusters (AuVCs) as nanozymes that enables the detection of a few molecules with the naked eye and quantified by an auto-analysis software. The GSH level controls the growth of gold nanoparticles (AuNPs) and generates coloured patterns with distinct tonality, which are then auto-analyzed to calculate the GSH concentrations by smartphone with an auto-analysis software. Under the optimized conditions, grayscale value plotted against GSH concentration exhibited a linear relationship within the range of 25–500 µM with a limit of detection (LoD) of 9.80 µM and highly positive correlation between detected GSH level and TMZ drug-resistance level in GBM cells. This excellent property allowed our approach to be used for on-site determination of GSH levels in a rapid (i.e., within 30 min), simple (i.e., auto-analysis software), and cost-effective process (i.e., instrument-free) for cancer precision therapy.

Keywords: Glioblastoma (GBM); drug resistance; glutathione detection; lateral flow strip; plasmonic signal; nanozymes.

1. Introduction

Glioblastoma multiforme (GBM) is highly proliferative, invasive, and difficult to completely resect through surgery. The median survival of patients with GBM is shorter than fifteen months, and less than 5% of patients with GBM survive longer than three years (Hamilton et al. 2014). At present, only two standard drugs, temozolomide (TMZ) and bis-chloroethyl nitrosourea (BCNU), exert antitumor activities in patients with GBM after surgery. However, their efficacy remains unsatisfactory because of intrinsic drug resistance, such as a decrease in cell uptake, intracellular drug inactivation, repair of drug-induced damage, and resistance to drug-induced apoptosis (Jiang et al. 2012; Pang et al. 2019a). Therefore, identifying and predicting the drug-resistance level of GBM cells might be helpful in precision GBM therapy for improving the treatment efficacy and prognosis of GBM. Glutathione (GSH) is the most abundant biothiol molecule; it is a crucial agent in cells' redox status, can prevent them from toxic molecules or mutagens, and has been proven to play a key role in drug resistance against DNA alkylating agents, especially TMZ, BCNU, and cisplatin (Bansal and Simon 2018; Byun et al. 2005; Rocha et al. 2014; Traverso et al. 2013). GSH plays a critical role in intracellular redox balance by participating in antioxidation systems to balance oxidative stress and many metabolic processes (Wu et al. 2004). The oxidative stress in cells has been considered a vital influencing factor in cancer progression and development in many studies. It has been demonstrated that the level of intracellular GSH is closely related to responsiveness to TMZ or cisplatin treatment. Thus, the cells with intrinsically high level of GSH might overcome attacks by therapeutic agents. (Ali-Osman et al. 1997; Bansal and Simon 2018; Tcherkas and Denisenko 2001). Zhu et al. have demonstrated the GSH content in GBM cells related to TMZ resistance, the cells with higher intracellular GSH content are more resistant to TMZ than the cells with normal level of GSH (Zhu et al. 2018). Rocha et al. demonstrated that GSH depletion will make GBM cells more

sensitive to cisplatin and TMZ both *in vitro* and *in vivo* (Rocha et al. 2014). Byun et al. also demonstrated that downregulate the GSH concentration using buthionine sulphoximine would augment the cisplatin sensitivity in bladder cancer cells (Byun et al. 2005).

Although there are many studies have indicated the relationship between GSH and drug resistance, to our knowledge, there are no specific golden-standard cut-off for the intracellular GSH concentration or content ratio. In addition, the detection of GSH level in cells or tissue still complicated and expensive. At present, the main methods of detecting GSH include high-performance liquid chromatography (HPLC) (Tcherkas and Denisenko 2001; Yuan and Edwards 2011), enzyme-linked immunosorbent assay (ELISA), electrochemistry (Xu et al. 2015; Zhu et al. 2015), and fluorescent analysis methods (Dai et al. 2016; Liu et al. 2017). However, these methods have many limitations. For example, HPLC requires expensive equipment (more than tens of thousands of US dollars), professional operators that make it difficult to achieve by labs or customers with fewer resources. The ELISA or enzyme reagent-based assays are prone to subjective errors, require experienced operators and are time consuming (usually take more than 3 h) that are all not suitable for on-site GSH detection. Therefore, it is pertinent to explore a convenient (easy-to-use), rapid (within 30 min), reliable, and low-cost (less than five US dollars for each assay) diagnostic test for on-site GSH determination. Bioosensing systems (or biosensors) have been developed to improve the convenience, stability, and sensitivity of traditional procedures for sensing antigens and metabolic molecules.

In this study, we circumvent the problems by introducing a plasmonic signal generation mechanism for rapid GSH detection with the naked eye based on lateral flow plasmonic biosensor (LFPB) comprising gold-viral biomineralized nanoclusters (AuVCs) and lateral flow strip. The GSH level controls the growth of gold nanoparticles (AuNPs) in the presence of AuVCs and generates coloured pattern in the detection area of LFPB, which is then auto-

analyzed to calculate the GSH concentrations by smartphone with an auto-analysis software. To our knowledge, this is the first study to on-site evaluate the drug-resistance level by instrument-free intracellular GSH biosensing using a LFPB with plasmonic signal. This AuVCs-based lateral flow plasmonic biosensing system has high sensitivity, selectivity, lower cost for on-site evaluation of drug-resistance level in cancer cells in laboratories or clinical usage in the future.

2. Material and methods

2.1. Materials

Phosphate-buffered saline (PBS, pH=7.4), L-glutathione reduced (CAS: 70-18-8), Isopropyl-β-D-thiogalactoside (IPTG, CAS: 367-93-1,), Streptomycin sulfate salt (CAS: 3810-74-0,), Ammonium sulfate (CAS: 7783-20-2,), Polyethylene glycol 8000 (PEG8000, CAS: 25322-68-3), Sucrose (CAS: 57-50-1), Sodium hydroxide (CAS: 1310-73-2), Tetrachloroauric(III) acid trihydrate (CAS: 16961-25-4) were purchased from Sigma-Aldrich (St. Louis, MO, USA). Difco™ LB brith (Luria Bertani) was purchased form fisher scientific. The TMB/H2O2 substrate (commercial) and it's stop solution were purchased from GeneDireX, Taiwan. The commercial reduced glutathione (GSH) assay kit (Colorimetric) was obtained from BioVision, Inc (155 S Milpitas Blvd. Milpitas, CA, USA).

2.2. Qβ virus-like particles (VLPs) bioproduction

In the present study, the VLPs bioproduction and purification procedures were as described in previous works (Fang et al. 2016, Pang et al. 2019a). In brief, plasmid vectors containing Qβ coat protein genome (pCDF–QβCP) were transformed to *E. coli* (BL21) and expression after isopropyl β-D-1-thiogalactopyranoside (IPTG) induction. In *E. coli*, the QβCPs would self-assemble into VLPs. The VLPs containing *E. coli* cells were harvested by

centrifugation and lysed by sonication. After several steps of protein purification, including ammonium sulfate precipitation, PEG8000/NaCl precipitation, and 2-butanol-chloroform extraction, the VLPs were sent for sucrose-gradient ultracentrifugation before phosphate-buffered saline (PBS) dialysis was performed. Finally, the VLPs were concentrated through protein concentrate filter tubes (Amicon Ultra-15 Centrifugal Filter Units; 100,000 MWCO; Merck Millipore, LOT: R6EA45140, Ireland) and qualified using a Pierce™ BCA Protein Assay kit (Thermo Scientific™, LOT: PD202250, USA).

2.3. Synthesis of AuVCs and bovine serum albumin (BSA)-gold nanoclusters (BSA-AuNCs)

Purified VLPs were resuspended in PBS buffer (pH = 7.4) and the concentration was adjusted to 3 μM. In brief, a freshly prepared aqueous solution of hydrogen tetrachlorocuprate hydrate ($HAuCl_4 \cdot 4H_2O$, 0.8 mM, 100 μL) was mixed with 100 μL of VLPs (3 μM) or BSA (3 μM) PBS solution before 0.1M NaOH solution (10 μL) was added. The solution was incubated in darkness at 37□ for 48 h. The crude product was dialyzed using a 10,000 MWCO dialyzing bag in PBS (pH = 7.4) for 24 h and stood in darkness for another 24 h for precipitation to obtain AuVCs or BSA-AuNCs. The supernatant was removed and the AuVCs concentrations were measured using the Pierce™ BCA Protein Assay kit.

2.4. Transmission electron microscope (TEM)

VLP-based samples were prepared by pipetting appropriate 5 μL of VLPs or AuVCs solution onto Formvar-coated copper mesh grids (200 mesh; Ted Pella, Redding, CA, USA) for 5 min, followed by being exposed to 8 μL of a solution of uranyl acetate (15 mg/mL in DI-H_2O) for 2 min as a negative stain. Subsequently, excess stain was removed and the grids were left to dry in air overnight. Next, the samples were analyzed using TEM (CM-200

TWIN instrument, Philips Co., Netherlands) with 75 keV accelerating voltage evaluation of diameter and morphology.

2.5. Ultracentrifugation imaging

The VLP-based samples (green fluorescent protein [GFP] packaging VLPs [gVLPs] and AuVCs) from the aqueous layer were purified using step sucrose gradient (10–40 wt% sucrose from top to bottom) ultracentrifugation at 40,000 rpm and 4□ for 135 min using an SW41 rotor. Subsequently, fluorescence images were captured under Dark Reader® Blue Transilluminator (Clare Chemical Research, USA) excitation by camera.

2.6. Fluorescence imaging of AuVCs

The purified AuVCs and VLPs were suspended in PBS buffer (pH = 7.4) and adjusted to 1 μM. Light imaging was conducted under a white light LED, and a fluorescence image was captured under UV light excitation at 320 nm. The purified AuVCs and VLPs were suspended in PBS buffer (pH = 7.4) and adjusted to 1 μM. Next, 100 μL of the samples were placed in a 96-well plate and the Fluorescence spectra were measured using a SpectraMax® M2 multimode plate reader (Molecular devices, LLC, USA).

2.7. Kinetic parameters of AuVCs toward TMB/H_2O_2

The kinetic parameters of AuVCs were studied using the initial rate method with the Michaelis constant. AuVCs was reacted with various concentrations of TMB (2.5, 5, 12.5, 30, and 50 μM) at 25°C in the presence of H_2O_2 to calculate the K_m and V_{max} values; V_{max} is the highest possible reaction velocity when AuVCs were saturated with TMB, and K_m is the Michaelis constant, which is the substrate concentration that yields half the true maximum reaction velocity; it represents the effective affinity between AuVCs and TMB. The results

were processed into a Lineweaver–Burk (1/S vs. 1/V) plot and the V_{max} and K_m values were calculated.

2.8. Preparation of lateral flow plasmonic strip

The lateral flow plasmonic strips were prepared by printing the designed pattern on filter papers (Grade 1 Qualitative Filter Paper Standard Grade, Whatman®) using Xerox colorcube 8570 wax printer (CQ8570, Xeron, USA). The lateral flow plasmonic strips were then incubated at 160°C for 3 min to melt the wax. Finally, the lateral flow plasmonic strips were cooled to room temperature and dried before use.

2.9. GSH detection using LFPB

For GSH detection, 1.4 μL of $HAuCl_4$ (100 mM) were dropped in the Y zone of the strip and dried at room temperature. Then 1 μL of AuVCs (1 μM) were mixed with 9 μL sample (i.e., GSH standard or cell lysates diluted with PBS buffer, pH = 6) and incubated at 37□ for 20 min followed by addition of 30 wt% H_2O_2 (5 μL) as the working solution. Afterward, the working solution were dropped onto the S zone of the strip and let the solution flow through the Y zone to X zone. After 5 min of running, the strip was dried at 37□ then put in the imaging box for image capture by smartphone. The greyscale value at detection zone (Y zone) was analyzed using auto-analysis software for massive data analysis to quantify the GSH concentration. The details of automatic image processing for GSH auto-analysis are described in the supplementary method section (Figure S1).

2.10. Stability investigation of LFPB

To investigate the stability of LFPB for intracellular GSH determination, the prepared LFPB were stored at room temperature for over 51 days in dark. The detection signal was

measured by the described procedure at different time points (day 0, 2, 20, 34, 41 and 51) using the auto-analysis software with same condition of $HAuCl_4$ concentration and H_2O_2 concentration. The greyscale values at Y zone were calculated in average and standard deviation as error bar (n=3).

2.11. Anti-interference and recovery investigations

An outstanding biosensor should possess not only accuracy but also specificity. Therefore, interference studies were performed on proposed LFPB. A variety of substances were employed, such as GSH (500 µM), cysteine (500 µM), cystamine (500 µM), PRO-PREP™ cell lysing buffer (100X dilution with PBS), IgG (10 ng/mL), DNA (plasmid DNA as sample, 1 mg/mL), cell extracted total RNAs (1 mg/mL) and BSA (1 wt%). The specificity of LFPB was determined by recording the greyscale value at Y zone according to abovementioned procedures.

For recovery studies, cell lysis buffer spiked with various concentrations of GSH (100, 220, 360 and 430 µM) then the spiked samples were analysed using LFPB according the operation procedures to determine the GSH concentrations. The recovery rate and relative standard deviation (RSD) were calculated using following equations:

$$Recovery(\%) = \frac{GSH\ concentration\ measured\ by\ LFPB}{Known\ sample\ GSH\ concentration} \times 100\% \qquad \text{(equation 1)}$$

$$RSD(\%) = \frac{standard\ deviation\ of\ GSH\ concentration\ by\ LFPB}{average\ of\ GSH\ concentration\ detected\ by\ LFPB} \times 100\% \qquad \text{(equation 2)}$$

2.12. Cell experimental procedures

To compare the GSH concentrations in different cells, six GBM cell lines (U87MG, T98G, U118MG, A172, GL261 and RG2) with different drug-resistance levels against TMZ, were cultured in Dulbecco's Modified Eagle's Medium (DMEM) with 2.2 mg/mL of sodium

carbonate, 10% fetal bovine serum, 50 µg/mL of penicillin, and 50 µg/mL of streptomycin at 37°C. For drug-resistance studies against TMZ, GBM cells were seeded into a 96-well plate (approximately 5000 cells/well) and incubated for 24 h then treated with 0.6 mM TMZ for another 24 h. The culture medium was removed, and the cells were incubated in 120 µL of XTT solution for 2 h. Subsequently, 100 µL of XTT solution from each well was transferred to another 96-well counting plate. The survival of GBM cells at the various concentrations of TMZ was evaluated by absorption intensity at 450 nm using the SpectraMax M2.

For GSH detection, those GBM cell lines were detached from cultured dish using 0.25 % (v/v) of trypsin. Next, the cells were washed once with PBS buffer (pH = 7.4) and a total of 1.4 x 10^5 cells for each cell line were lysed using a PRO-PREP™ protein extraction kit (iNtRON biotechnology, CAT:17081.1, USA). Subsequently, the solution was placed in an ice bath for 5 min followed by centrifugation (2,500 rpm, 10 min) to remove cell debris. The supernatant was collected and transferred to a new tube for the GSH detection using GSH ELISA kit and proposed LFPB according to the abovementioned procedures.

2.13. Statistical analysis

The data were expressed as mean ± SD on the basis of at least three independent experiments. Statistical analysis was performed using a Student's *t* test; $*p < 0.05$ and $*p < 0.01$ were considered statistically significant.

3. Results and discussion

Scheme 1 presents the preparation of materials and principle of this detection method. The synthesized AuVCs exhibited high peroxidase activity which can control the oxidation of TMB or the growth of AuNPs for colour development depending on the GSH concentration. Thus, the working solution prepared by mixing AuVCs with GSH sample for 20 min,

followed by addition of TMB/H_2O_2 or $HAuCl_4$/H_2O_2. However, the TMB is easily oxidized to exhibited interference with obvious colour background; thus, we designed a new plasmonic signal generation combined with a lateral flow strip to determine the intracellular GSH concentration. As the concentration of GSH increased, the peroxidase activity of AuVCs toward H_2O_2 was also reduced. Afterward, the prepared working solution was dropped onto S zone of the strip with 2-D computational recognition guiding lines. The solution would flow through Y zone and control the growth of AuNPs at Y zone of the strip to exhibit deep purple color. The strip was then put in an imaging box for image capture by smartphone and the greyscale value of Y zone was automatically calculated using customized software for evaluation of GSH concentration.

3.1. Production and characterization of VLPs and AuVCs

First, the VLPs were prepared through bioproduction in *Escherichia coli* (*E. coli*) according to the method used in our previous studies (Pang et al. 2019a; Pang et al. 2019b) and described in the method section 2.2. AuVCs were formed using a facile one-step chemical reduction of $HAuCl_4$ in alkaline solution with VLPs as a template. Photographs were captured after the VLPs had reacted with $HAuCl_4$ for 48 h in alkaline solution. The solution became yellowish and displayed red fluorescence under illumination with an ultraviolet (UV) light (λ_{max} = 320 nm) compared with VLPs only (Figure 1A). The prepared AuVCs exhibited a shoulder absorption at approximately 400 nm in the UV-vis absorption spectrum (Figure 1B), which could be attributed to discrete electronic states arising from the ultra-small size of the AuNCs. The resultant AuVCs exhibited intense red fluorescence with a maximum peak at approximately 650 nm under UV light irradiation (Figure 1C). The morphology of VLPs and AuVCs were first characterized using transmission electron microscopy (TEM); no obvious difference in morphology was observed between them, but

the diameter of the AuVCs was slightly decreased to 26.50 ± 0.80 nm compared with VLPs (28.90 ± 0.90 nm). This was most likely because the formed AuNCs made the coat proteins more tightly assembled with Au–S bonds (Figure 1D). During energy dispersive x-ray spectroscopy (EDS), a new Au (12.9 wt%) signal belonging to AuNCs appeared after the growing of AuNCs on coat protein of VLPs was compared with VLPs. Subsequently, the synthesized AuVCs were purified using ultracentrifuge sucrose gradient purification; they displayed red fluorescence and were located at the same position as the VLPs (Figure 1E). In addition, we compared the efficiency of AuNCs formation using VLPs as template (AuVCs) with that using BSA as template (BSA-AuNCs) under same synthesis process. The results demonstrated that significant fluorescence was observed in AuVCs group compared with BSA-AuNCs group, indicating that much more AuNCs were grown on the VLPs than BSA (Figure S2A). This might because VLPs having a stable 3D structure for clusters growing, leading faster formation of AuNCs on VLPs than BSA. Previous studies have demonstrated that VLPs could benefit the mineralization of metal ions due to the amino acid residues or the cage-like structure and the mineralization could improve the stability or catalysis efficiency in the 3-D structure of VLPs capsid assembly (Stark et al. 2017; Schwarz et al. 2017; Du et al. 2019). We also did the comparison of TMB/H_2O_2 catalytic oxidation efficiency between AuVCs and BSA-AuNCs (synthesized by same parameters as AuVCs), the AuVCs can catalyze TMB/H_2O_2 to produce more yellow oxidation product with a significant absorbance at 450 nm than BSA-AuNCs (Figure S2B). We also investigated the reproducibility of AuVCs by preparing 5 batches of AuVCs using same protocol and parameters on different days (one batch per day) (Figure S3). The peroxidation activity of those AuVCs was analysed by reacting with TMB/H_2O_2 and measuring the $A_{450\ nm}$, and no significant difference in the $A_{450\ nm}$ was observed between each batch of fabrication, indicating that the fabrication process of AuVCs is very stable. Taken together, these observations indicated that the

synthesis of AuNCs using VLPs as a template was highly efficient, and the AuNCs were indeed integrated into VLPs to form AuVCs.

3.2. Kinetics and stability studies of AuVCs

In this study, we observed synthesized new AuVCs as an artificial peroxidase, which replaced HRP for catalyzing the oxidation of TMB in the presence of H_2O_2, producing a yellow oxidation product with a significant absorbance at 450 nm (Figure 2A). There is no reaction while wild-type VLPs were mixed with TMB/H_2O_2 solution (Figure S4) which means that the catalytic ability is caused by gold cluster in VLPs not the viral coat proteins. The kinetic parameters V_{max} and K_m of the AuVCs were assayed by reacting the AuVCs with different concentrations of TMB in the presence of constant H_2O_2 and were calculated from Lineweaver–Burk plots (Figure 2B). The V_{max} of the AuVCs was 5.75 ± 0.43 μM/min, which was slightly lower than the value for HRP (6.60 ± 0.30 μM/min) (Aumiller et al. 2014). This was most likely because the steric effects caused by coat proteins of the VLPs hindered the approach of the TMB/H_2O_2 to the active AuNCs. By contrast, the K_m values for TMB and AuVCs (41.67 ± 4.51 μM) were lower than that of the HRP (100 ± 10 μM) (Aumiller et al. 2014). The affinity between the catalyst (AuVCs or HRP) and TMB decreased as the K_m value increased. These results indicated that the affinity between AuNCs on AuVCs and TMB/H_2O_2 increased compared with HRP, which may result from the 3D structure of AuVCs being able to pull inside the AuVCs, the inferred mechanism is similar to the previous study reported by Fiedler et al. (Fiedler et al. 2018). Alternatively, this could attract more TMB/H_2O_2 onto the coat proteins through the pores of the coat protein shell by electrostatic attraction, thereby increasing the frequency of collision between AuNCs on AuVCs and TMB/H_2O_2.

Most relevant literature has indicated high peroxidation activity of HRP in a weak acid environment based on a TMB/H_2O_2 oxidation reaction, and the optimal activity was obtained under a pH value of 6 (Peng et al. 2019); however, this may not suit all biomolecules. Thus, the influence of pH (4 to 11) was investigated to determine the peroxidation activity for AuVCs. The results in Figure 2C demonstrate that the peroxidation activity was not affected by pH; the artificial enzyme AuVCs could effectively oxidize TMB in the presence of H_2O_2 to obtain a consistent signal over a wide pH range from 4–11, indicating that AuVCs are more suitable than HRP for the analysis of clinical samples. The greatest concern in enzyme-based biosensors is their lack of stability, which is caused by the intrinsic nature of the enzyme. Therefore, we further evaluated the long-term stability of HRP and AuVCs after a period of storage between 1 and 21 days at 25 and 37□; the responses were monitored by reacting TMB with the HRP and AuVCs stored at each time point in the presence of H_2O_2. The HRP lost its complete activity after 4 days of storage at 25 and 37□; however, the AuVCs were used for oxidizing TMB in the presence of H_2O_2 without any loss in catalytic activity, even when stored at 25 and 37□ for 21 days (Figure 2D). The activity of AuVCs did not decrease but increased with increasing incubation temperatures; this might because the assembly of coat proteins became looser at higher temperatures to reduce the steric effects between them and AuNCs, which can promote the collision of AuNCs on AuVCs with TMB/H_2O_2 to enhance peroxidation. The results indicated that AuVCs are more suitable than HRP as a peroxidase in any storage and detection environments, which would be advantage for further applications.

3.3. Colorimetric GSH detection using AuVCs through TMB/H_2O_2

In conventional colorimetric biosensing, a signal is generated by the conversion of the colourless enzyme substrate (i.e., TMB) into a coloured molecule then recorded by measuring

the absorbance intensity using a spectrometer to determine the concentration of target molecule. The GSH could be detected by inhibiting the peroxidation activity of AuVCs toward the TMB/H_2O_2 in the presence of GSH. According to previous reports, we proposed three biosensing mechanisms of AuVCs for GSH detection in this study: (1) GSH strongly binds with Au atoms on the surface of AuVCs through Au–S bonds (Zhang et al. 2018) to decrease collisions between H_2O_2 and AuVCs and generate ·OH radicals; (2) GSH can scavenge ·OH radicals arising from the decomposition of H_2O_2 (Feng et al. 2017); and (3) the coat protein shell of AuVCs is disassembled through interruptions to the disulfide bond in the presence of GSH. To confirm the proposed mechanisms, we investigated the structure and peroxidation activity of AuVCs after incubation with a certain amount of GSH. After the VLPs were incubated with various concentrations of GSH solution for approximately 0.5 h, their diameters in solution increased from 31.50 ± 0.70 nm to 41.30 ± 0.90 (Table S1 and Figure S5) measured by dynamic light scattering, indicating that disulfide bonds for VLP assembly can be interrupted to cause instability of AuVC structures (Chen et al. 2018; Cheng et al. 2018). In addition, SDS-PAGE was used to confirm that the VLPs had been disassembled to pentamers and hexamers (the molecular weight of a VLP coat protein monomer is 14.4 kDa) after 0.5 h of incubation with 100 mM 2-mercaptoethanol (BME) (Figure S6, lane 1) or 5 mM GSH (Figure S6, lane 2) compared with VLPs without any treatment (Figure S6, lane 4). No obvious disassembly of coat proteins was observed when the VLPs were incubated with 0.5 mM GSH (Figure S6, lane 3), indicating that only high concentrations of GSH can disassemble the coat protein shell; specifically low concentrations of GSH cannot effectively interrupt enough disulfide bonds to collapse the VLPs. Therefore, under optimized conditions, the AuVCs were used to detect the concentration of GSH. The color of the solutions clearly changed from dark to light yellow in the presence of GSH, and the color became lighter when the concentration of GSH increased, which could be

distinguished by the naked eye. According to the results in Figure S7A, the absorption intensity at 450 nm ($A_{450\ nm}$) decreased when the concentration of GSH gradually increased. $A_{450\ nm}$ plotted against GSH concentration was linear within a range of 1–500 μM with a correlation coefficient of 0.993 (Figure S7B). This result indicated that GSH concentration-dependent inhibition of the peroxidation activity of AuVCs toward TMB/H_2O_2 for GSH determination. However, the poor water solubility of TMB and requirement of stop solution both limit the application of colorimetric biosensing.

3.4. Plasmonic signal generation mechanism

In our approach, the prepared AuVCs can be the template to allow AuNPs growth on their surface as plasmonic signal for determination of GSH concentration by the control of AuNPs growth. In the proposed method, the AuVCs would be collapsed by GSH to reduce the formation of AuNPs. As in Figure 3A, a AuNPs surface plasmon resonance (SPR) peak at 540-550 nm observed only in the presence AuVCs, $HAuCl_4$ and H_2O_2 but the SPR peak disappeared when the GSH was added to collapse AuVCs. These results indicate that the AuVCs act as catalysts and templates for the reduction of $AuCl_4^-$ by H_2O_2, resulting in the growth of the AuNPs, and the GSH concentration can be determined by monitoring the level of AuNPs formation. To further understand if the HRP have similar ability to catalyze the AuNPs formation, we also performed another assay to figure out such question as shown in Figure S8. Only AuVCs could induce the AuNPs formation in the presence of $HAuCl_4/H_2O_2$, and the concentration of AuNPs formation depends on the concentration of AuVCs. The results support the abovementioned mechanism, the prepared AuVCs not only can reduce $AuCl_4^-$ in the presence H_2O_2 but also be a template for AuNPs growth.

3.5. GSH determination using LFPB

For instrument-free and rapid detection of intracellular GSH, we designed a new lateral flow strip with 2-D computational recognition lines and three zones: loading zone (S), detection zone (Y) and control zone (X). The working solution was prepared by mixing constant AuVCs with various concentrations of GSH at 37□ for 20 min followed by addition of 5 μL of 30 wt% H_2O_2. Afterward, the working solution was dropped on S zone and flowing through Y zone to X zone in 30 sec. The strip was then put in an imaging box containing stable LED light for image capture using a smartphone. As shown in Figure 3B, obvious AuNPs formation to exhibit deep purple color at Y zone when the AuVCs-included working solution flowed through Y zone compared with AuVCs-excluded working solution. The results were also confirmed by scanning electron microscope (SEM), lots of small particles were formed and accumulated on fibers at Y zone of the lateral flow strip when the AuVCs-included working solution dropped on the S zone (Figure 3B, right). Conversely, the fibers showed very smooth when the AuVCs-excluded working solution dropped on the S zone (Figure 3B, left).

As the concentration of GSH increased, the formation of AuNPs at Y zone decreased (Figure 4A), resulting in the greyscale value recorded by smartphone and calculated by customized software was increased. The standard curve was found to be linear in the range of 25 to 500 μM with a limit of detection (LoD) of 9.80 μM (r^2 = 0.986, Figure 4B). Furthermore, we also try to investigate the detection ability of GSH using TMB/H_2O_2 as signal substrate in this LFPB system. The results showed that the TMB can be oxidized to display blue colour while the AuVCs flowed through Y zone but the oxidized TMB (blue colour) spread to the channel between X and Y zones because the molecular weight of TMB is too small to stay in Y zone (Figure S9), resulting in difficult signal recording. Therefore,

the proposed plasmonic signal with AuNPs formation may be more suitable for utility in this lateral flow paper based biosensor.

To prove the specificity and accuracy of the proposed LFPB toward GSH detection, we studied whether GSH, natural amino acids, and proteins will affect the formation of AuNPs or not. As shown in Figure 4C, the interferences (including lysis buffer, BSA, DNA, RNAs, IgG, cysteine and cystamine) all would not affect the formation level of AuNPs to cause significant change of greyscale value at Y zone compared with that of blank at Y zone, whereas a distinct greyscale value change was observed in the presence of same concentration of GSH, cysteine and cystamine. However, the intracellular concentration of GSH is a thousand times higher than that of cysteine, cystamine or other thiols (Li et al. 2017; Niu et al. 2015; Tian et al. 2014); thus the interferences of cysteine and cystamine would not happen during intracellular GSH detection. To further confirm the accuracy of LFPB for GSH determination, we spiked various concentrations of GSH (100, 220, 360 and 430 μM) into lysis buffer and performed the GSH determination using LFPB by recording the greyscale value at Y zone. The recovery rates of intracellular GSH concentration were found to be acceptable and in the range of 99.64–104.71% and the relative standard deviations were all lower than 3.5%, indicating that the proposed LFPB comprising a lateral flow strip and plasmonic signal generation mechanism is accurate enough for instrument-free intracellular GSH determination without any interferences. In addition, we also investigated the storage stability of AuVCs for a period of 51 days, there was no significant decrease in greyscale value at Y zone observed (Figure S10) when the AuVCs (1 μM) stored for each time period were reacted with a constant concentration of GSH (50 μM).

3.6. Intracellular GSH determination using a LFPB

As one of most critical physiological parameters for cancer cells with different levels of drug-resistance, the differences in GSH content induced by the alteration of redox status would provide a substantial predictive index for discriminating them, as well as greatly aid in devising appropriate treatment strategies such as combination therapies with other chemotherapeutics. Thus, a convenient and rapid method for on-site intracellular GSH determination plays a pivotal role. In this study, we selected the human GBM cell lines (T98G, U87MG, A172, U118MG, RG2 and GL261) with different levels of drug-resistance as the model and used the proposed LFPB to determine their GSH concentrations on-site. The cell lysates were immediately mixed with AuVCs for 20 min followed by addition of H_2O_2 as the working solution, which was then dropped on the S zone of the lateral flow strip. Their GSH concentrations (264.68 ± 5.25 μmole/g for U118MG, 197.26 ± 13.63 μmole/g for GL261, 264.68 ± 5.25 μmole/g for U87MG, 427.02 ± 7.07 μmole/g for A172, 612.84 ± 0.28 μmole/g for RG2 and 648.78 ± 11.63 μmole/g for T98G) were determined by recording the greyscale values at Y zone using smartphone auto-calculation. The obtained results were also compared with those obtained using the GSH assay kit, and no significant difference was found between them (Figure 5A), demonstrating the excellent accuracy and reliability of the LFPB for detecting GSH in real cell samples. To identify the correlation between drug-resistance level and intracellular GSH concentration, six GBM cell lines with different drug-resistance level were treated with 0.6 mM of TMZ for 24 h. As shown in Figure 5B, almost cultured RG2, T98 and A172 cells survived (cell viability: 98.13 ± 0.38 % for RG2 cells, 96.82 ± 1.14 % for T98 cells, 88.43 ± 1.85 % for A172 cells) after being treated with 0.6 mM TMZ while their intracellular GSH concentrations were all higher than 400 μmole/g. By contrast, relatively many U87MG, U118MG and H4 cells were killed by treatment with same conditions (cell viability: 74.22 ± 3.94 % for U87MG cells, 55.64 ± 3.45 % for U118MG cells, 64.97 ± 4.72 % for H4 cells), this result may be attributed to the lower concentration of

GSH expression (were all lower than 300 μmole/g) in these cells. Correlation coefficient of the intracellular GSH concentration to the cell viability is 0.855 (*p*-value = 0.03), indicating the correlation between GSH content and cell viability is positive. A notable trend was found, GSH concentrations increased as the cell viability increased after treatment with TMZ. The results indicating that the cells with higher intracellular GSH expression may exhibit greater TMZ drug-resistance than did the cells with lower intracellular GSH expression. We also performed the GSH determination in three tumor tissue samples from three GBM patients without TMZ drug-resistance (according to *O*-6-methylguanine-DNA methyltransferase test) using LFPB, the detected GSH concentrations were 70~120 μmole/g. The obtained results were also compared with those obtained using the GSH assay kit, and no significant difference was found between them (Figure 5C). Our approach possesses some distinct advantages in terms of its ease of operation, time saving (total processing time = approx. 30 min), low-cost characteristics (requires only lateral flow strip and microliters of reagents, the cost estimated to be less than 1 USD), and high durability compared with the commercial GSH assay kit (total processing time = approx. 180 min). With the commercial kit, many solutions should be freshly prepared with specific pretreatment, carefully and immediately used, and stored under strict conditions. By contrast, the proposed LFPB would offer a straightforward and reliable approach for accurately evaluating cellular GSH levels to assess whether the cell is a cancer cell with high or low drug-resistance or a normal cell by automatic calculation using smartphone and online software. The detail comparison between other GSH detection methods and our approach in this work in Table S2.

Conclusions

In summary, we developed a new LFPB comprising a lateral flow strip and AuVCs to control the generation of plasmonic signal depending on the GSH concentration for instrument-

free and on-site intracellular GSH determination to identify the drug-resistance level of cancer cells, especially those with main resistance mechanisms related to GSH in cells. This approach endowed GSH determination with operational simplicity, convenient readouts, and high stability, and furthermore, it was capable of evaluating the intracellular GSH concentration; here, it was found that intracellular GSH concentrations in cancer cells with high drug-resistance were much higher than those in cancer cells with low drug-resistance. To our knowledge, this is the first report on viral nanocluster development with high catalyzation activity for AuNPs formation and achieve GSH evaluation in complex biosystems such as cells by combination of LFPB based online auto-analyzing system. We envisage that this strategy has great potential as a potent tool for clinical diagnosis, therapy related to GSH, and even strategy designs for combination therapy.

Conflicts of interest

There are no conflicts to declare.

Acknowledgments

This work was financially supported by the Ministry of Science and Technology and National Health Research Institutes, Taiwan (ROC), whom we thank for the financial assistance provided (MOST106-2628-E-110-001-MY3, MOST106-2628-B-110-MY4, MOST108-2314-B-182-019-MY2, CORPG3I0111, NHRI-EX108-10502NI). Furthermore, we would like to thank the Chang Gung Memorial Hospital Microscopy Core Laboratory for their TEM and SEM assistance.

References

Ali-Osman, F., Brunner, J.M., Kutluk, T.M., Hess, K., 1997, Clin. Cancer Res. 3, 2253-2261.

Aumiller, W.M., Jr., Davis, B.W., Hatzakis, E., Keating, C.D., 2014, J. Phy. Chem. B. 118, 10624-10632.

Bansal, A., Simon, M.C., 2018, J.Cell Bio. 217, 2291-2298.

Byun, S.S., Kim, S.W., Choi, H., Lee, C., Lee, E., 2005, BJU Int. 95, 1086-1090.

Chen, G., Ma, B., Wang, Y., Gong, S., 2018, ACS Appl. Mater. Interfaces 10, 18515-18523.

Cheng, Q., Yin, H., Sun, C., Yue, L., Ding, Y., Dehaen, W., Wang, R., 2018, Chem. Commun. 54, 8128-8131.

Dai, X., Du, Z.F., Wang, L.H., Miao, J.Y., Zhao, B.X., 2016, Anal. Chim. Acta. 922, 64-70.

Du, P., Liu, R., Sun, S., Dong, H., Zhao, R., Tang, R., Dai, J., Yin, H., Luo, J., Liu, Z., Guo, H., 2019, Nanoscale 11, 22748-22761.

Feng, J., Huang, P., Shi, S., Deng, K.Y., Wu, F.Y., 2017, Anal. Chim. Acta. 967, 64-69.

Fiedler, J.D., Fishman, M.R., Brown, S.D., Lau, J., Finn, M.G., 2018, Biomacromolecules 19, 3945-3957.

Hamilton, J.D., Rapp, M., Schneiderhan, T., Sabel, M., Hayman, A., Scherer, A., Kropil, P., Budach, W., Gerber, P., Kretschmar, U., Prabhu, S., Ginsberg, L.E., Bolke, E., Matuschek, C., 2014, J. Clin. Oncol. 32, e80-84.

Jiang, G., Li, L.T., Xin, Y., Zhang, L., Liu, Y.Q., Zheng, J.N., 2012, Curr. Med. Chem. 19, 3886-3892.

Li, S.S., Guan, Q.Y., Zheng, M., Wang, Y.Q., Ye, D., Kang, B., Xu, J.J., Chen, H.Y., 2017, Chem. Sci. 8, 7582-7587.

Liu, C., Qi, F., Wen, F., Long, L., Yang, R., 2017, Methods Appl. Fluoresc. 6, 024001.

Niu, L.Y., Chen, Y.Z., Zheng, H.R., Wu, L.Z., Tung, C.H., Yang, Q.Z., 2015, Chem. Soc. Rev. 44, 6143-6160.

Pang, H.H., Huang, C.Y., Chou, Y.W., Lin, C.J., Zhou, Z.L., Shiue, Y.L., Wei, K.C., Yang, H.W., 2019a, Nanoscale 11, 8102-8109.

Pang, H.H., Chen, P.Y., Wei, K.C., Huang, C.W., Shiue, Y.L., Huang, C.Y., Yang, H.W., 2019b, Theranostics 9, 1752-1763.

Peng, C., Hua, M.Y., Li, N.S., Hsu, Y.P., Chen, Y.T., Chuang, C.K., Pang, S.T., Yang, H.W., 2019, Biosens. Bioelectron. 126, 581-589.

Rocha, C.R., Garcia, C.C., Vieira, D.B., Quinet, A., de Andrade-Lima, L.C., Munford, V., Belizário, J.E., Menck, C.F., 2014, Cell Death Dis. 5, e1505.

Schwarz, B., Uchida, M., Douglas, T., 2017, Adv. Virus. Res. 97, 1-60.

Stark, M.C., Baikoghli, M.A., Lahtinen, T., Malola, S., Xing, L., Nguyen, M., Nguyen, M., Sikaroudi, A., Marjomäki, V., Häkkinen, H., Cheng, R.H., 2017, Sci. Rep. 7, 17048.

Tcherkas, Y.V., Denisenko, A.D., 2001, J. Chromatogr. A. 913, 309-313.

Tian, M., Guo, F., Sun, Y., Zhang, W., Miao, F., Liu, Y., Song, G., Ho, C.L., Yu, X., Sun, J.Z., Wong, W.Y., 2014, Org. Biomol. Chem. 12, 6128-6133.

Traverso, N., Ricciarelli, R., Nitti, M., Marengo, B., Furfaro, A.L., Pronzato, M.A., Marinari, U.M., Domenicotti, C., 2013, Oxid. Med. Cell. longevity. 2013, 972913-972913.

Wu, G., Fang, Y.Z., Yang, S., Lupton, J.R., Turner, N.D., 2004, J. Nutr. 134, 489-492.

Xu, H., Xiao, J., Liu, B., Griveau, S., Bedioui, F., 2015, Biosens. Bioelectron. 66, 438-444.

Yuan, W., Edwards, J.L., 2011, J. Chromatogr. A 1218, 2561-2568.

Zhang, X., Chen, X., Jiang, Y.W., Ma, N., Xia, L.Y., Cheng, X., Jia, H.R., Liu, P., Gu, N., Chen, Z., Wu, F.G., 2018, ACS Appl. Mater. Interfaces 10, 10601-10606.

Zhu, W., Jiang, G., Xu, L., Li, B., Cai, Q., Jiang, H., Zhou, X., 2015, Anal. Chim. Acta 886, 37-47.

Zhu, Z., Du, S., Du, Y., Ren, J., Ying, G., Yan, Z., 2018, J. Neurochem. 144, 93-104.

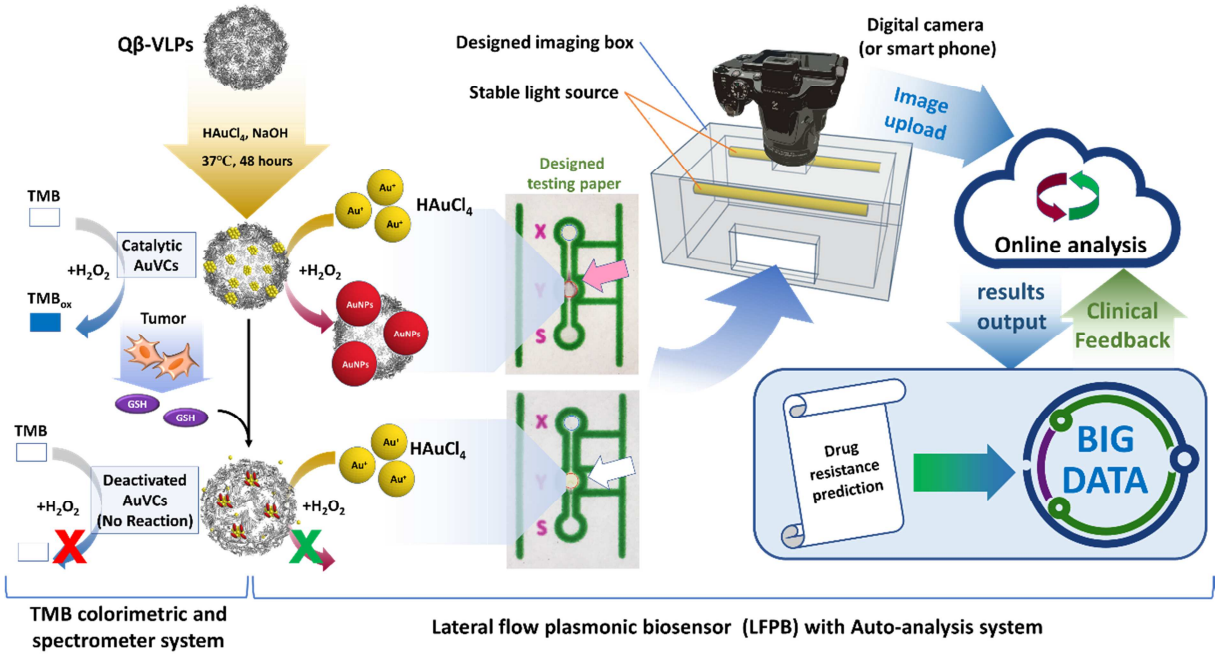

Scheme 1. The overview design and procedures of this study. Qβ-VLPs were co-incubated with $HAuCl_4$ and NaOH to generate AuNCs. The formed AuVCs are GSH sensitive and could catalyze the formation of AuNPs in presence of $HAuCl_4$ and H_2O_2. The deactivation of AuVCs caused the catalysis ability decrease lead to the poor yield of AuNPs formation. Designed testing paper containing recognition lines and flow-detection zones were printed using wax printer. The sample could be analyzed using image box with smartphone or digital camera then sent to the online auto-analyzing software. The output data could help prediction of drug resistance and for big data analysis to improve the prediction accuracy.

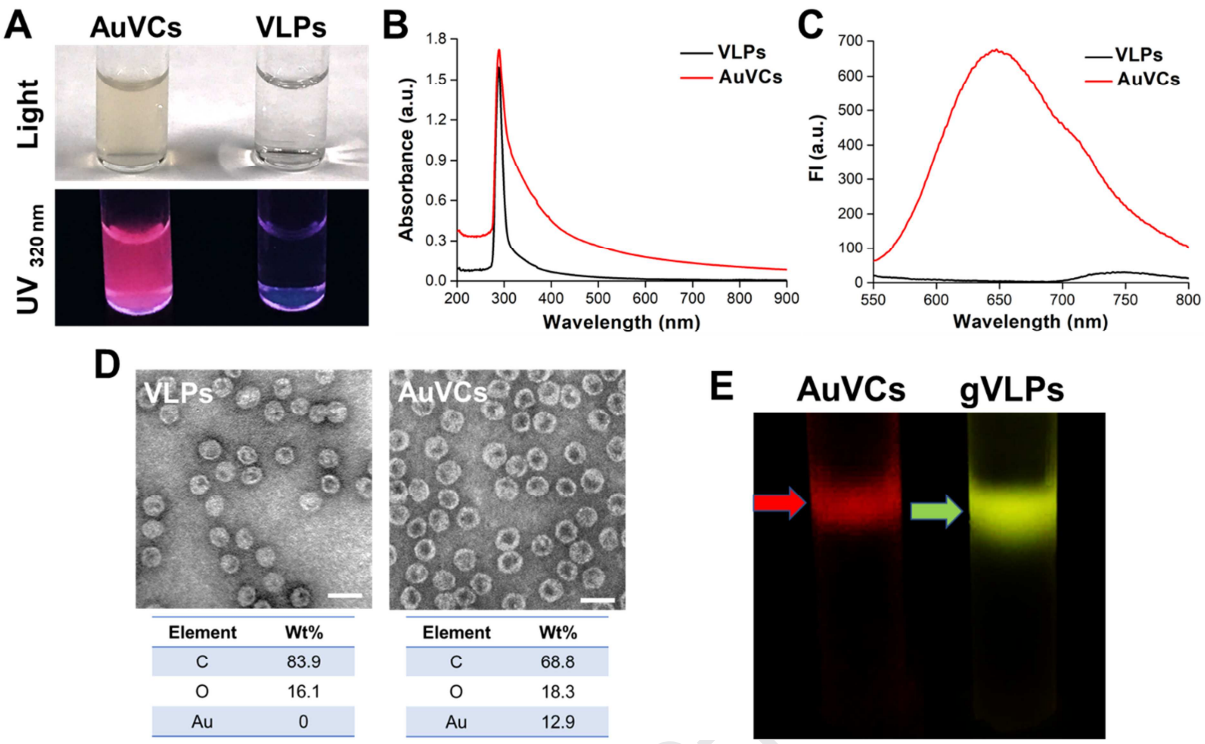

Figure 1. Characterizations of AuVCs. (A) White light photograph (top) and fluorescence photograph (bottom) under UV light excitation (wavelength = 320 nm) of VLPs and AuVCs. (B) UV-vis absorption spectra of VLPs and AuVCs. (C) Fluorescence spectra of VLPs and AuVCs at an excitation wavelength of 320 nm. (D) TEM images of VLPs (left) and AuVCs (right). Scale bar = 100 nm. (E) Fluorescent image of gVLPs (right) and AuVCs (left) under Darkreader® excitation after sucrose gradient ultracentrifugation.

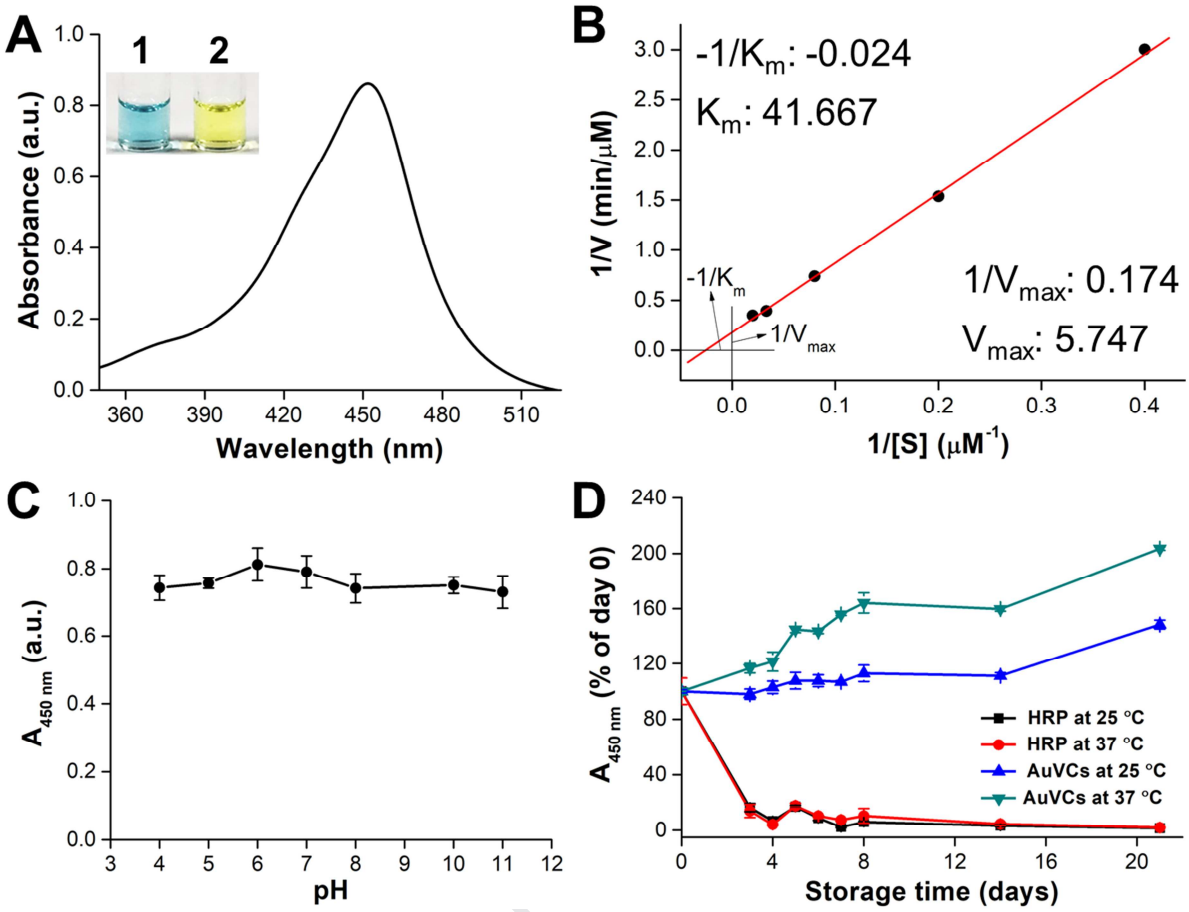

Figure 2. (A) UV-vis absorption spectrum of TMB in the presence of 1 μM AuVCs after addition of stop solution (1M HCl). The inset is the photograph of TMB in the presence of 1 μM AuVCs (1) before addition of stop solution and (2) after addition of stop solution. (B) The Lineweaver–Burk (1/S vs. 1/V) plot of AuVCs was analyzed by reacting AuVCs with TMB in the presence of H_2O_2. (C) Absorbance of AuVCs at 450 nm in the presence of H_2O_2 + TMB in PBS with different pH levels. Values are expressed as means ± SD (n = 6). (D) Stability of HRP and AuVCs stored at 25 and 37°C for a period of 0–21 days. The AuVCs showed no decrease in oxidizability toward H_2O_2 + TMB after 21 days of storage at 37°C. Values are expressed as means ± SD (n = 6).

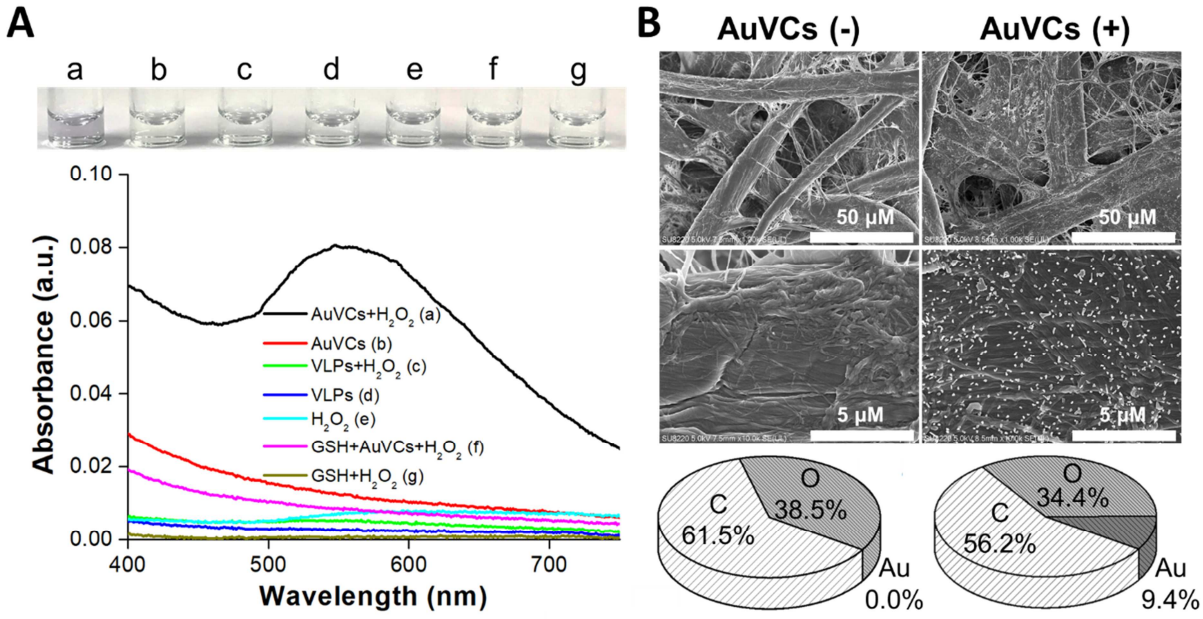

Figure 3. (A) The UV-Vis absorbance spectra for $HAuCl_4$ reacted with different groups and corresponding photographs. (B) SEM images of LFPB at Y zone while the working solution containing AuVCs or not, and the corresponding EDS analysis.

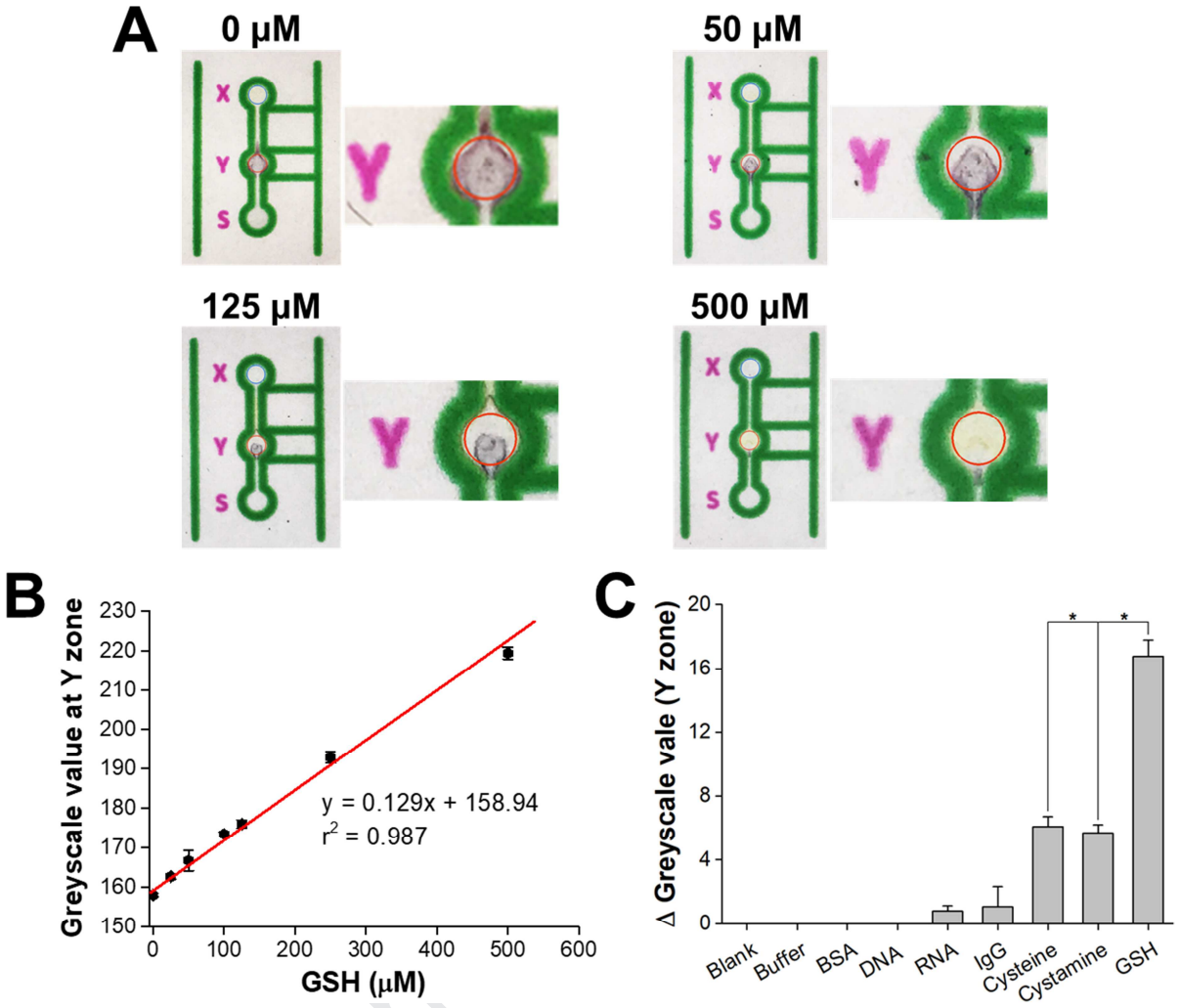

Figure 4. (A) Photographs of LFPB after dropping of the working solution containing various concentrations of GSH (0, 50, 125 and 500 μM) on S zone. The red circles are automatically selected by the auto-analysis software to determine the GSH concentration. (B) Linear calibration curve of GSH with different concentrations determined by LFPB. Values are expressed as means ± SD (n = 3). (C) Specificity tests of LFPB for intracellular GSH determination with various interferences. Values are expressed as means ± SD (n = 3). *indicates a significant difference (Student's *t*-test, *$p \leq 0.05$).

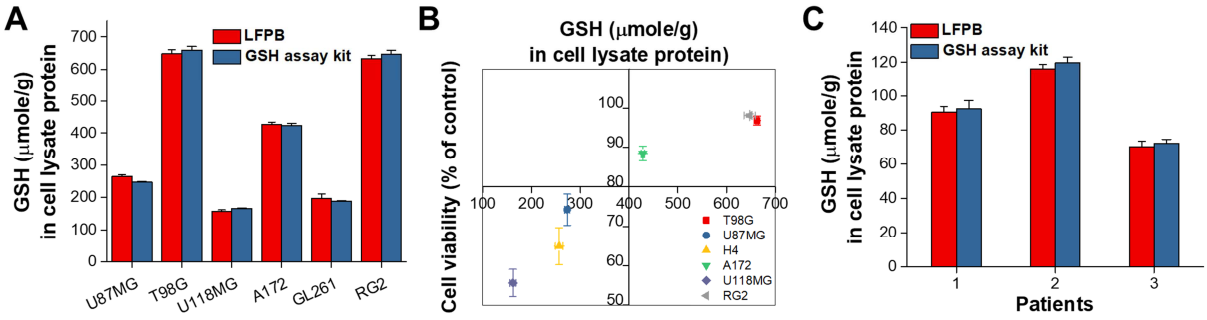

Figure 5. (A) Intracellular GSH concentration of various species of GMB cell lines measured via commercial GSH assay kit (blue) and LFPB (red). Values are expressed as means ± SD (n = 3). Values are expressed as means ± SD (n = 3). (B) Correlation between cell viability (treated with 0.6 mM TMZ for 24 h) and intracellular GSH concentration (measured LFPB) in unit (μmole/g cell lysate protein). Values are expressed as means ± SD (n = 6). (C) GSH concentration in tumor tissue protein lysates extracted from three different patient's GBM tumor tissue measured by LFPB or GSH assay kit. Values are expressed as means ± SD (n = 3). All three groups having no significant difference between LFPB and GSH assay kit (Student's t-test, p=0.733 for patient 1, p=0.126 for patient 2, p=0.598 for patient 3).

Table 1. Recovery tests of GSH spiking using LFPB.

Spiked (μM)	Average detected concentration (μM)	recovery (%)	RSD (%)
100	100.72 ± 0.41	100.72	0.41
220	230.35 ± 7.37	104.71	3.2
360	369.42 ± 9.76	102.62	2.64
430	428.47 ± 14.38	99.64	3.36

Values are expressed as means ± SD (n = 3)

Highlights

- Gold-viral biomineralized nanoclusters (AuVCs) with high peroxidability and stability as artificial peroxidase.
- A new lateral flow plasmonic biosensor (LFPB) for on-site glutathione (GSH) determination.
- The easy-to-use LFPB combined with smartphone could achieve a limit of detection of 9.8 μM and a wide range of 25–500 μM for GSH.
- This LFPB offers a straightforward and reliable approach for accurately evaluating drug-resistance levels.

Conflicts of interest

There are no conflicts to declare.